The Astrophysical Journal, 675:553–565, 2008 March 1

OBSERVATION OF AN UNEXPECTED HARDENING IN THE SPECTRUM OF GRB 021206

C. Wigger,[1,2] O. Wigger,[2] E. Bellm,[3] and W. Hajdas[1]

Received 2007 July 9; accepted 2007 November 12

ABSTRACT

GRB 021206 is one of the brightest GRBs ever observed. Its prompt emission, as measured by *RHESSI*, shows an unexpected spectral feature. The spectrum has a peak energy of about 700 keV and can be described by a Band function up to 4.5 MeV. Above 4.5 MeV, the spectrum hardens again, so the Band function fails to fit the whole *RHESSI* energy range up to 17 MeV. Nor does the sum of a blackbody function plus a power law, even though such a function can describe a spectral hardening. The cannonball model, on the other hand, predicts such a hardening, and we found that it fits the spectrum of GRB 021206 perfectly. We also analyzed other strong GRBs observed by *RHESSI*, namely, GRBs 020715, 021008, 030329, 030406, 030519B, 031027, and 031111. We found that all their spectra can be fit by the cannonball model, as well as by a Band function.

Subject headings: gamma rays: bursts — gamma rays: observations — techniques: spectroscopic

1. INTRODUCTION

The exact mechanism which produces γ-ray bursts (GRBs) has not yet been definitively established. Their prompt γ-ray spectra can be used to distinguish between different models. Several mathematical functions have been used for parameterizing the prompt γ-ray emission. Most commonly used is the empirical Band function (Band et al. 1993), which is not motivated by a physical model.

There have been attempts to distinguish between spectral models analyzing the low-energy part of the spectrum. Ghirlanda et al. (2003), Ryde (2004), and more recently Ghirlanda et al. (2007) searched for blackbody components in GRB spectra with varying degrees of success. Preece et al. (2002), using BATSE GRB spectra, tested the synchrotron shock model and conclude that it "does not account for the observed spectra during the GRB phase."

Spectral studies above the peak energy are rare, one reason being the poor data quality because of lack of statistics. Combining BATSE and EGRET spectra, González et al. (2003) report a high-energy component for GRB 941017. They find a photon index of about 1.0 at energies above 5 MeV.

In this paper we report a high-energy component in GRB 021206 (Hurley et al. 2002e, 2002f, 2003b), observed with the *Reuven Ramaty High-Energy Solar Spectroscopic Imager* (*RHESSI*; Lin et al. 2002). Having a peak energy of about 700 keV, the spectrum of this burst can be described by a Band function from 70 keV up to 4.5 MeV, with a high-energy photon index $\beta \approx 3.2$. Above 4.5 MeV, the spectrum hardens again and can be described with a photon index $\beta' \approx 2.2$. This significant hardening around 4.5 MeV cannot be described with a Band function. However, it seems to differ from the spectral hardening in GRB 941017 as well.

There is one model that fits the entire *RHESSI* spectrum of GRB 021206: the cannonball model (Dar & de Rújula 2004; Dado et al. 2002, 2003a). The cannonball model predicts a spectral hardening at several times the peak energy with a high-energy photon index reaching $\beta \approx 2.1$.

[1] Paul Scherrer Institut, CH-5232 Villigen PSI, Switzerland.
[2] Tellistrasse 9, CH-5000 Aarau, Switzerland.
[3] UC Berkeley Space Sciences Laboratory, 7 Gauss Way, Berkeley, CA 94720-7450.

The question immediately arises whether the cannonball model can improve our description of other GRB spectra. The difference between the Band function and the cannonball model arises only at the high-energy part of the spectrum, where data usually suffer from low statistics. Therefore, we choose the strongest GRBs registered by *RHESSI* in the years 2002–2004. We find that they all can be fit by the cannonball model, as well as by the Band function.

The outline of the paper is the following: We first briefly present the instrument, the GRB selection, the spectrum extraction, and the fit method (§ 2). In the next section (§ 3), many spectral functions are given. In § 4, the fit results for GRB 020715, GRB 021008, GRB 021206, GRB 030329, GRB 030406, GRB 030519B, GRB 031027, and GRB 031111 are presented. The fits are discussed and, if possible, compared to other measurements. The more general discussion, including the prospects for future research, follows in § 5. We end with a short summary in § 6.

2. INSTRUMENT AND METHOD

2.1. *Instrument*

RHESSI is a NASA Small Explorer mission designed to study solar flares in hard X-rays and γ-rays (Lin et al. 2002). It consists of two main parts: an imaging system and the spectrometer with nine germanium detectors (Smith et al. 2002). The satellite always points toward the Sun and rotates about its axis at 15 rpm. The Ge detectors are arranged in a plane perpendicular to this axis.

The shape of the detectors is cylindrical with a height of $\approx$8.5 cm and diameter of $\approx$7.1 cm, and they are segmented into a thin front ($\approx$1.5 cm) and a thick rear segment ($\approx$7 cm). Since the shielding of the rear segments is minimal, photons with more than about 25 keV can enter from the side. Above about 50–80 keV, photons from any direction can be observed. Each detected photon is time and energy tagged from 3 keV to 2.8 MeV (front segments) or from 20 keV to 17 MeV (rear segments). The energy resolution is $\approx$3 keV at 1 MeV, and the time resolution is 1 μs.

The effective area for GRB detection depends on the incident photon energy E and the angle between the GRB direction and the *RHESSI* axis, the incoming angle θ. Over a wide range of E and θ, the effective area is around 150 cm^2. The sensitivity drops rapidly at energies below $\approx$50 keV.

TABLE 1
GRB Analysis Time Intervals

GRB	t_0 (UT)	$\Delta t_{\rm burst}$ (s)	$\Delta t_{\rm BG1}$ (s)	$\Delta t_{\rm BG2}$ (s)	θ (deg)	References
020715	19:20:56.0	[11.53, 15.55]	[−80.46, 0.0]	[48.28, 168.97]	72.4	1, 2
021008	07:00:45.0	[17.21, 21.29]	[−73.37, 0.0]	[36.68, 48.91]	50.1	3, 4
021206	22:49:11.7	[2.73, 8.19]	[−53.26, 0.0]	[20.49, 102.43]	18.0	5, 6
030329 P1	11:37:10.0	[16.56, 24.84]	[−70.39, 0.0]	[70.39, 140.78]	144.1	7
030329 P2	11:37:10.0	[28.98, 34.50]	[−70.39, 0.0]	[70.39, 140.78]	144.1	7
030406	22:41:30.0	[85.68, 89.83]	[−140.96, 0.0]	[140.96, 281.93]	96.1	8
030519B	14:04:53.0	[0.46, 11.47]	[−61.94, 0.0]	[28.90, 90.84]	165.5	9, 10
031027	17:07:06.0	[29.71, 45.92]	[−137.77, 0.0]	[68.88, 206.65]	101.5	11
031111	16:45:12.0	[2.27, 6.35]	[−122.51, 0.0]	[12.25, 134.76]	155.6	12

Notes.—t_0: reference time; $\Delta t_{\rm burst}$: time interval for spectral analysis; $\Delta t_{\rm BG1}$: background time interval before GRB; $\Delta t_{\rm BG2}$: background time interval after GRB; time intervals are given relative to t_0. The angle between GRB direction and *RHESSI* axis is θ; References: (1) GCN 1454 (Hurley et al. 2002a; (2) GCN 1456 (Hurley et al. 2002b); (3) GCN 1617 (Hurley et al. 2002c; (4) GCN 1629 (Hurley et al. 2002d); (5) GCN 1727 (Hurley et al. 2002e; (6) GCN 1728 (Hurley et al. 2002f); (7) GCN 1997 (Vanderspek et al. 2003); (5) GCN 2127 (Hurley et al. 2003a); (9) GCN 2235 (Lamb et al. 2003); (10) GCN 2237 (Hurley et al. 2003c); (11) GCN 2438 (Hurley et al. 2003d); (12) *HETE* trigger 2924, GCN 2443 (Hurley et al. 2003e).

2.2. *GRB Selection*

For this study, we need well-observed GRB spectra. We chose GRBs from the years 2002–2004 because radiation damage starts to play a role in 2005. The selected GRBs have to be localized by other observations of the same GRB (*RHESSI* cannot measure the incoming angle), because θ enters into the simulation of the response function. A further requirement was the availability of good background data. And finally, the data-storing mode ("rear decimation" for onboard memory saving) is not allowed to change during the entire GRB and background time interval. Of all the GRBs meeting these criteria, we chose eight with the best signal-to-background ratio, listed in Table 1 along with their incoming angle θ and the time intervals used. The light curves of these bursts are shown in Figures 1 and 2.

2.3. *Preparation and Fit of RHESSI Spectra*

The method of analyzing *RHESSI* GRB spectra will be described in detail in a separate article (E. Bellm, et al. 2008, in preparation). For each GRB and detector segment, the total spectrum (GRB plus background) during the burst was extracted, as well as the background spectra during two time intervals before and after the burst. The background was linearly (sometimes quadratically) interpolated and subtracted. The exact time intervals are listed in Table 1. Then we added all rear and all front segments, except for detector 2, which is slightly damaged and has a bad energy resolution. Since all GRBs in this study are strong, the observational errors are dominated by the statistical error of the GRB counts, not of the background.

We simulate *RHESSI* using GEANT3 (CERN 1993). Knowing the direction of the GRB from other instruments, we simulate *RHESSI*'s response to photons coming from angle θ. The energy of the incoming photons is simulated as a power-law spectrum (i.e., $dN/dE \propto E^{-\gamma_{\rm sim}}$) with typically $\gamma_{\rm sim} = 2$.

This power-law simulation is only a rough approximation and is not intended to represent the intrinsic GRB spectrum, but instead provides simulated data representing *RHESSI*'s conversion of photons to counts. The true GRB source spectrum is determined via weight factors for the resulting simulated count spectrum, as described below. The upper energy limit of the simulated photon spectrum is typically 30 MeV, in the case of GRB 021206 even 40 or 50 MeV. This is important because an incoming photon of, e.g., 25 MeV may well make a signal of 15 MeV. Rotation angles are generated uniformly; i.e., we compute a *RHESSI* spin-averaged response function. Since the detector arrangement shows an approximate 120° symmetry, the averaging gives good results as long as the analyzed time interval is at least one-third of the rotation period ($T_{\rm rot} = 4$ s). This was also confirmed by tests.

The output of the simulation is an event list, or rather a hit list, consisting of all signals registered in the Ge detectors. The simulated hit list, having N_s entries indexed by the letter l, contains the deposited energy ($E_l^{\rm det}$), as well as the initial photon energy ($E_l^{\rm in}$). The measured hit list contains only the observed energy.

For spectral fitting, the observed energy histogram is compared with a histogram accumulated from the simulated hit list. More precisely: The measured histogram can be represented by a k-element vector $\boldsymbol{M}$ with errors $\boldsymbol{\sigma}_M$ and energy boundaries E_0^b, E_1^b, E_2^b, ..., E_k^b. We normalize the histogram $\boldsymbol{M}$ to the total number of counts in the fit range: $\boldsymbol{m} = \boldsymbol{M}/C_M$ and $\boldsymbol{\sigma}_m = \boldsymbol{\sigma}_M/C_M$, where $C_M = \sum_{i \in I} M_i$ and the sum goes only over the bins included in the fit, i.e., $I = \{i \mid \text{bin } i \text{ is included in the fit}\}$. The "theoretical" histogram $\boldsymbol{S}$ is accumulated from the simulated hit list.

Each entry is weighted with a factor in order to scale from the simulated power law to the probability density which would be expected had we actually simulated the GRB source spectrum dN/dE. The jth bin contains therefore the weighted sum of all simulated hits with $E_l^{\rm det}$ belonging to that bin, i.e.,

$$S_j = \sum_{l \in L} w_l, \tag{1}$$

where $L = \{l \mid E_{j-1}^b \le E_l^{\rm det} < E_j^b\}$ and

$$w_l = \left(\frac{E_l^{\rm in}}{E_{\rm piv}}\right)^{\gamma_{\rm sim}} \frac{dN}{dE}(E_l^{\rm in}). \tag{2}$$

The first factor in equation (2) accounts for the spectrum assumed in the simulation, and the energy $E_{\rm piv}$ is an arbitrary normalization. The second factor accounts for the spectrum of the incoming GRB photons. Possible parameterizations of dN/dE are given below in § 3. If the GRB spectrum had the same shape as the simulated one, i.e., if $dN/dE = (E/E_{\rm piv})^{-\gamma_{\rm sim}}$, the weights would all be 1. This method of using weight factors when filling a histogram is common in particle physics (see, e.g., Barlow & Beeston 1993). The statistical error of the theoretical histogram $\boldsymbol{S}$ is $\sigma_{S_j}^2 = \sum_{l \in L} w_l^2$ (§ 6 of Barlow & Beeston 1993).

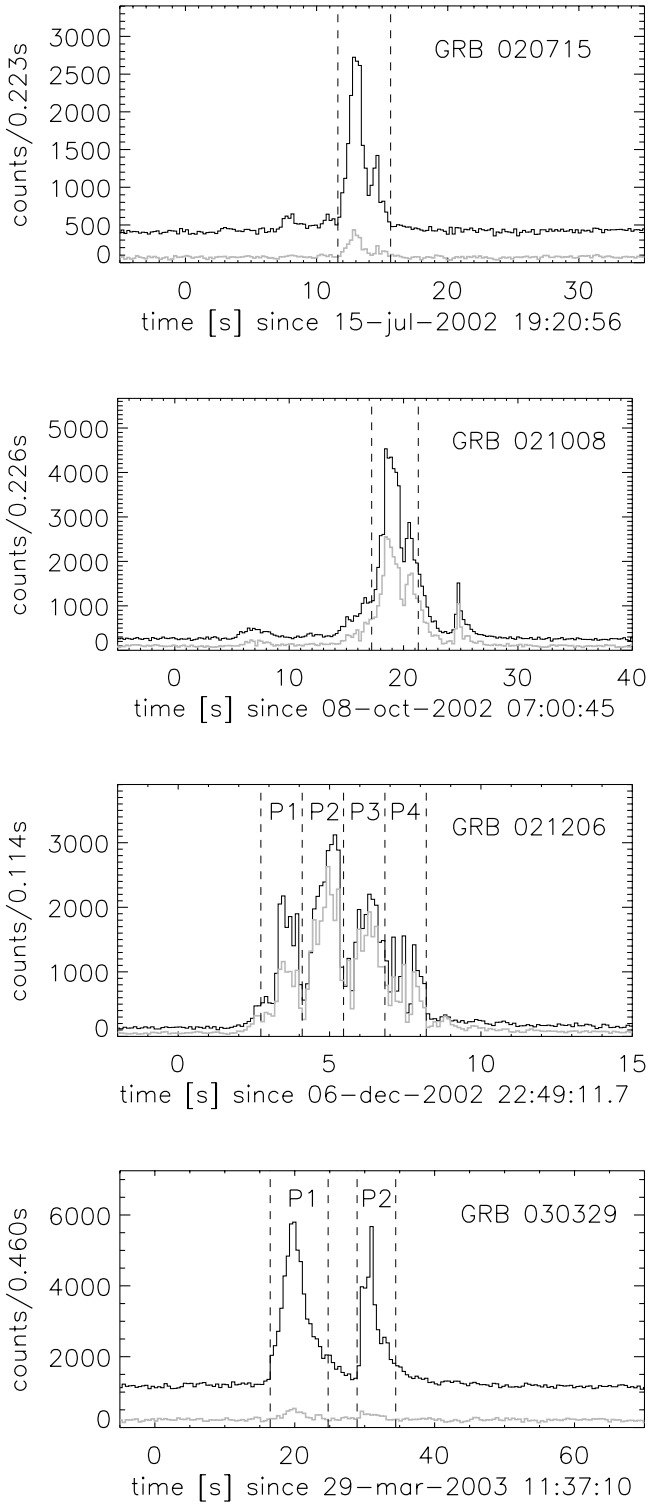

FIG. 1.—Light curves for the energy band of 20 keV to 3 MeV; *black*: rear detectors; *gray*: front detectors; *vertical dashed lines*: time intervals used for spectral analysis.

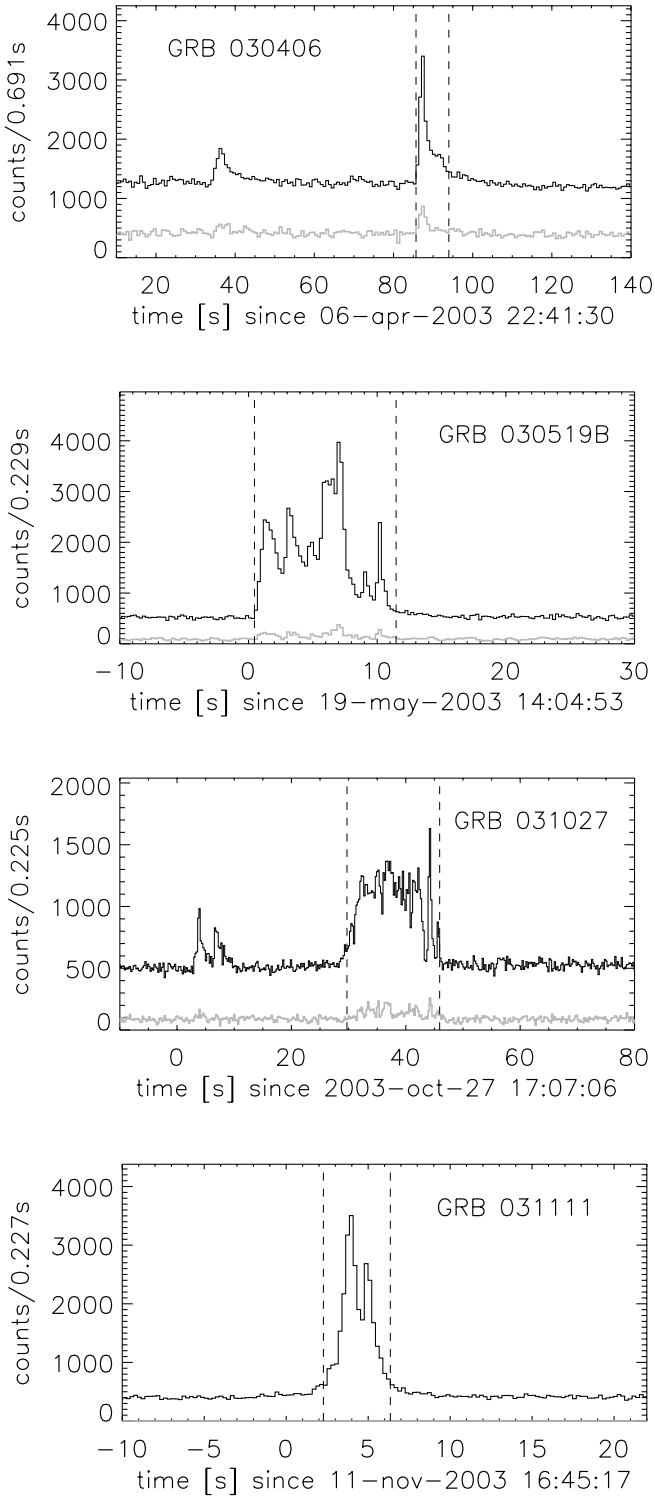

FIG. 2.—Same as Fig. 1.

As in the case of the measured histogram, the histogram $\boldsymbol{S}$ is normalized: $\boldsymbol{s} = \boldsymbol{S}/C_S$ and $\boldsymbol{\sigma}_s = \boldsymbol{\sigma}_S/C_S$ with $C_S = \sum_{i \in I} S_i$.

The parameters of the histogram $\boldsymbol{S}$ are varied until the minimum of

$$\chi^2 = \sum_{i \in I} \frac{(m_i - f s_i)^2}{\sigma_{m_i}^2 + \sigma_{s_i}^2} \tag{3}$$

is found. The factor f accounts for the normalization between measured and simulated histograms. It is expected to be almost 1 but should be treated as a free fit parameter. For each fit iteration, the histogram $\boldsymbol{S}$ is recalculated with different weights (eq. [2]).

Since the simulated hit list contains many more photons than the measured spectrum, we used the approximation $\sigma_{m_i}^2 + \sigma_{s_i}^2 \approx \sigma_{m_i}^2$ while fitting. But it was always checked that the statistical error from the measurement is dominant.

It is possible to create a response matrix from our simulations and perform spectral fits via forward fitting, as in XSPEC. In

any case, our weighted histogram method gives equivalent fits to response matrices which are simulated directly (see E. Bellm et al. 2008, in preparation).

2.4. *Systematic Effects*

At low energies, a small deviation of our *RHESSI* mass model from the true amount of material can make a considerable difference in the number of observed photons. For $\theta \approx 90^\circ$, this should be a small problem because the lateral shielding is thin. But for θ from 10° to 50° this is an issue, and less prominently also from 130° to 160°.

Simulation quality also gets better with higher energy. This is fortunate for the current analysis, which relies on high-energy properties of GRB spectra.

3. SPECTRAL MODELS

Let dN/dE be the number of GRB photons per energy bin. The peak energy $E_{\rm peak}$ is defined as the energy for which $EF_E = dN/dEE^2$ is maximal. The spectrum in the EF_E representation has at least one maximum because the total emitted energy must be finite: $\int_0^\infty dN/dE\, E\, dE < \infty$. Many instruments can see such a maximum $E_{\rm peak}$ within their energy range.

Different mathematical functions, sometimes called models, can describe such a shape. A collection is presented in this section.

The simplest spectral function is a power law (PL):

$$\frac{dN}{dE} = A\left(\frac{E_{\rm piv}}{E}\right)^{\gamma}, \tag{4}$$

where $E_{\rm piv}$ is a normalization energy, e.g., $E_{\rm piv} = 100$ keV. The PL has no peak energy. It rarely fits a GRB spectrum over the entire observed energy range, but it is often useful for a limited energy band. Indeed, every spectrum can be fit by several joined PLs.

One simple way to account for a spectral softening and a peak energy is the cutoff power law (CPL):

$$\frac{dN}{dE} = A\left(\frac{E_0}{E}\right)^{\alpha} e^{-E/E_0}. \tag{5}$$

If $\alpha < 2.0$, then $E_{\rm peak} = E_0(2-\alpha)$.

Another way to account for a spectral break is the broken power law (BPL), consisting of two joined PLs

$$\frac{dN}{dE} = \begin{cases} A\left(\dfrac{E_b}{E}\right)^{\alpha} & \text{if } E \le E_b, \\ A\left(\dfrac{E_b}{E}\right)^{\beta} & \text{if } E \ge E_b. \end{cases} \tag{6}$$

If $\alpha < 2.0$ and $\beta > 2.0$, then $E_{\rm peak} = E_b$. This function is not continuously differentiable.

A smooth transition between the two power laws is realized by the empirical Band function (Band et al. 1993). This is a smooth composition of a CPL for low energies and a PL for high energies:

$$\frac{dN}{dE} = \begin{cases} A\left(\dfrac{E_{\rm piv}}{E}\right)^{\alpha} e^{-E/E_0} & \text{if } E \le E_{\rm break}, \\ B\left(\dfrac{E_{\rm piv}}{E}\right)^{\beta} & \text{if } E \ge E_{\rm break}, \end{cases} \tag{7}$$

where

$$E_{\rm break} = E_0(\beta - \alpha)$$

and

$$B = A\left[\frac{E_0}{E_{\rm piv}}(\beta-\alpha)\right]^{\beta-\alpha} e^{-(\beta-\alpha)}.$$

Again, $E_{\rm piv}$ is a normalization energy, e.g., $E_{\rm piv} = 100$ keV. If $\alpha < 2.0$ and $\beta > 2.0$, then $E_{\rm peak} = E_0(2-\alpha)$. If $\beta \longrightarrow \infty$ or if $E_{\rm break}$ lies at the upper limit of the observed energy range, then the Band function turns into a CPL. As already pointed out by Preece et al. (2000, their § 3.3.1), the low-energy photon index, the curvature of the spectrum, and its peak energy are represented with only two parameters, α and E_0.[4]

Sometimes a blackbody spectrum plus power law is used for spectral fitting (see, e.g., Ryde 2004; Ghirlanda et al. 2007; McBreen et al. 2006). We call this the BBPL:

$$\frac{dN}{dE} = A\frac{[E/(kT)]^2}{\exp[E/(kT)]-1} + Ab\left(\frac{E_{\rm piv}}{E}\right)^{\alpha}. \tag{8}$$

We choose $E_{\rm piv} = 3.92kT$, the peak energy of the blackbody component. The BBPL function can fit a spectral hardening at high energies.

When fitting with the BBPL model, it is often found that the PL component does not fit simultaneously at low and at high energies. This is also mentioned by Ryde (2004). We therefore invented a blackbody plus modified power law (BBmPL):

$$\frac{dN}{dE} = A\frac{[E/(kT)]^2}{\exp[E/(kT)]-1} + Ab\left(1-e^{-E/E_0}\right)\left(\frac{E_0}{E}\right)^{\alpha}. \tag{9}$$

Again we choose $E_0 = 3.92kT$.

The modification of the power-law component was borrowed from the cannonball model (see next). The BBmPL function can describe a spectral hardening at high energies.

The cannonball model (CBM; Dar & de Rújula 2004; Dado et al. 2002, 2003a) makes a prediction for the spectral shape of the prompt GRB emission. It consists of a CPL and a modified power law:

$$\frac{dN}{dE} = A\left(\frac{T}{E}\right)^{\alpha} e^{-E/T} + Ab\left(\frac{T}{E}\right)^{\beta}\left(1-e^{-E/T}\right), \tag{10}$$

according to Dar & de Rújula (2004, their eq. [47]), or Dado et al. (2004, their eq. [13]). The theoretically expected values are $\alpha \approx 1.0$ and $\beta \approx 2.1$.

The CBM function equation (10) applies, strictly speaking, only to the spectrum caused by a single cannonball, i.e., for every single peak of a GRB.

It is often observed that the peak energy $E_{\rm peak}$ is a more stable fit parameter than the parameter E_0 in the Band function (eq. [7]) or in the CPL (eq. [5]). Therefore, we use $E_p = E_0(2-\alpha)$ as a fit parameter. Similarly, we use $T_p = T(2-\alpha)$ as a fit parameter in the case of CBM (eq. [10]).

A word about fitting CBM: For the high-energy part, it has two parameters, whereas the Band function has only one. Already when fitting the Band function, it is often observed that the

[4] The smoothly broken power-law model (SBPL; see Preece et al. 2000; Kaneko et al. 2006) would account for this problem with an additional parameter, but we do not use it here because it cannot fit a spectral hardening at high energies.

TABLE 2
χ^2 of Spectral Fits

GRB	$\Delta E_{\rm front}$ (keV)	$\Delta E_{\rm rear}$ (keV)	n	CPL $n_{\rm par}=3$	Band 4	CBM 4	CBM 5	BPL 4	BBPL 4	BBmPL 4
020715	...	[30, 15,660]	117	113.9	106.3	110.8	110.7	129.2	270.0	157.1
021008	[300, 2800]	...	38	35.5	34.8	35.1	35.0	33.0	32.9	33.9
021008	...	[300, 15,660]	50	43.8	39.2	39.9	39.2	52.9	97.4	60.2
021008	[300, 2800]	[300, 15,660]	88	...	79.5	80.8	...	...	...	...
021206	[70, 2800]	...	112	130.6	103.6	104.1	103.9	155.5	315.7	191.8
021206	...	[300, 16,000]	78	338.1	133.3	82.7	82.7	132.9	94.1	110.5
021206	[70, 2800]	[300, 16,000]	190	...	...	...	187.5	...	...	...
021206	...	[300, 4500]	66	...	72.8	69.8	...	...	...	...
021206	[70, 2800]	[300, 4500]	178	...	176.5	...	...	...	...	...
030329 P1	...	[34, 10,000]	94	86.5	84.3	84.8	84.7	89.3	137.8	89.1
030329 P2	...	[34, 7000]	87	104.5	103.3	103.2	103.1	98.9	102.0	98.4
030406	...	[24, 15,000]	75	79.1	75.6	75.0	75.0	88.6	151.2	88.7
030519B	...	[70, 15,000]	79	102.2	86.3	91.1	89.0	99.8	189.8	109.8
031027	...	[60, 6000]	63	63.6	n.c.	n.c.	n.c.	93.0	138.9	99.6
031111	...	[38, 15,000]	117	182.4	128.3	133.2	130.4	140.5	266.0	133.0

Notes.—The value of χ^2 was obtained by fitting different spectral models to the data. $\Delta E_{\rm front/rear}$: energy interval used to fit front/rear detector data; n: the number of energy bins; $n_{\rm par}$: number of free fit parameters; CPL: cutoff power law (eq. [5]); Band: Band function (eq. [7]); CBM: cannonball model (eq. [10]); BPL: broken power law (eq. [6]); BBPL: blackbody plus power law (eq. [8]); BBmPL: blackbody plus modified power law (eq. [9]); n.c.: fit did not converge. In the case of CBM with four parameters, β was fixed to its theoretically expected value of 2.1. For each fit the degree of freedom is $n_{\rm dof}=n-n_{\rm par}$.

high-energy power-law index is poorly constrained, because the high-energy data tend to have large statistical errors. This is even worse for CBM, with two high-energy parameters. It often helps to freeze the parameter β at its theoretical value of $\beta=2.1$ in order to make the fit converge.

4. FIT RESULTS AND FIT DISCUSSIONS

The spectral models used and the χ^2 of the fits are listed in Table 2 for all eight GRBs. For CBM and Band function, the fitted parameters are listed in Tables 3 and 4, respectively. Throughout this paper, all errors are symmetric 1 σ errors if not stated otherwise.

The measured spectra, together with the CBM and Band fits, are shown in Figures 3–13. Note that we do not plot a deconvolved EF_E distribution, but the measured counts keV^{-1} (after background subtraction) multiplied by the square of the measured energy. The difference to a deconvolved EF_E distribution is discernible, e.g., in the drop of counts toward lower energies in our representation. The statistical scatter from the limited number of simulated events is sometimes visible as a little roughness of the simulated spectra.[5]

From the fit parameters obtained for the CBM and the Band function, we calculate the fluences for various energy intervals. They are listed in Table 5. The error of the fluence is dominated by systematics, e.g., because we do not know the exact active volume of the single detector segments. We estimate the systematic error to be of the order of 5%, whereas the statistical error is of the order of 1%. Note also that the two fluences obtained by fitting CBM and the Band function are nearly equal.

[5] In the case of, e.g., GRB 021206, rear (see Fig. 7), the mean measured error between 4 and 12 MeV is 0.65×10^6 counts keV, whereas the mean scatter of the simulated histogram is 0.25×10^6 counts keV. For the other GRBs with fewer observed photons and therefore larger measurement errors, the statistical error of the simulation is even more negligible.

TABLE 3
Fit Results for CBM

GRB	$\Delta E_{\rm front}$ (keV)	$\Delta E_{\rm rear}$ (keV)	T_p (keV)	α	β	b
020715	...	[30, 15,660]	532 ± 20	0.741 ± 0.077	2.20 ± 0.14	0.067 ± 0.040
021008	[300, 2800]	...	628 ± 71	1.31 ± 0.28	2.1	0.052 ± 0.076
021008	...	[300, 15,660]	672 ± 68	1.487 ± 0.062	2.77 ± 0.55	0.085 ± 0.092
021008	[300, 2800]	[300, 15,660]	641 ± 32	1.523 ± 0.055	2.1	0.020 ± 0.008
021206	[70, 2800]	...	672 ± 20	0.66 ± 0.21	1.92 ± 0.67	0.063 ± 0.142
021206	...	[300, 16,000]	672 ± 24	0.67 ± 0.19	2.12 ± 0.13	0.102 ± 0.048
021206	[70, 2800]	[300, 16,000]	678 ± 6	0.60 ± 0.06	2.10 ± 0.08	0.103 ± 0.028
021206	...	[300, 4500]	670 ± 23	0.71 ± 0.15	2.1	0.091 ± 0.012
021206	[70, 2800]	[300, 4500]	...	...	...	...
030329 P1	...	[34, 10,000]	147 ± 10	1.614 ± 0.036	2.1	0.033 ± 0.029
030329 P2	...	[34, 7000]	69 ± 15	1.841 ± 0.049	2.1	0.048 ± 0.055
030406	...	[24, 15,000]	626 ± 83	0.966 ± 0.089	2.1	0.18 ± 0.12
030519B	...	[70, 15,000]	396 ± 12	0.949 ± 0.073	2.388 ± 0.097	0.135 ± 0.048
031027	...	[60, 6000]	340 ± 17	0.950 ± 0.055	2.1	−0.010 ± 0.025
031111	...	[38, 15,000]	690 ± 45	0.68 ± 0.27	2.241 ± 0.023	1.09 ± 0.36

Notes.—$\Delta E_{\rm front/rear}$: energy interval used to fit front/rear detector data; α, β, b: parameters as defined in eq. (10); $T_p=T(2-\alpha)$. Errors are symmetric 1 σ errors; where no error is given the parameter was frozen at that value.

TABLE 4
FIT RESULTS FOR BAND FUNCTION

GRB	$\Delta E_{\rm front}$ (keV)	$\Delta E_{\rm rear}$ (keV)	E_p (keV)	α	β
020715	...	[30, 15,660]	531 ± 24	0.776 ± 0.044	3.14 ± 0.25
021008	[300, 2800]	...	670 ± 58	1.36 ± 0.23	3.41 ± 0.51
021008	...	[300, 15,660]	678 ± 42	1.526 ± 0.067	3.86 ± 0.25
021008	[300, 2800]	[300, 15660]	677 ± 33	1.493 ± 0.056	3.73 ± 0.18
021206	[70, 2800]	...	713 ± 17	0.694 ± 0.031	3.20 ± 0.13
021206	...	[300, 16,000]	...	...	...
021206	[70, 2800]	[300, 16,000]	...	...	...
021206	...	[300, 4500]	709 ± 18	0.72 ± 0.20	3.186 ± 0.063
021206	[70, 2800]	[300, 4500]	711 ± 7	0.692 ± 0.020	3.19 ± 0.04
030329 P1	...	[34, 10,000]	157.2 ± 5.2	1.608 ± 0.038	3.48 ± 0.53
030329 P2	...	[34, 7000]	85 ± 11	1.781 ± 0.065	3.04 ± 0.30
030406	...	[24, 15,000]	674 ± 70	0.979 ± 0.064	2.61 ± 0.27
030519B	...	[70, 15,000]	417 ± 13	1.048 ± 0.042	3.11 ± 0.18
031027	...	[60, 6000]	338 ± 15	0.940 ± 0.079	...
031111	...	[38, 15,000]	844 ± 59	1.102 ± 0.036	2.364 ± 0.068

NOTES.—$\Delta E_{\rm front/rear}$: energy interval used to fit front/rear detector data; α, β: fit parameters in eq. (7); $E_p = E_0(2 - \alpha)$.Where no β is given a CPL (eq. [5]) was fitted; errors are symmetric 1 σ errors.

4.1. *GRB 020715*

The light curve is shown in Figure 1 (*top*), and the spectrum is shown in Figure 3. Two bins from 290 to 310 keV (a background line) and one bin from 500 to 525 keV (the 511 keV line) were omitted in the fit because they would dominate χ^2. The best fit is a Band function, but the CBM also fits well.

4.2. *GRB 021008*

Coming from a direction about 50° from the Sun, this GRB deposited photons not only in rear detectors but also in the front detectors, as can be seen from the light curve in Figure 1. The front spectrum is shown in Figure 4 and the rear in Figure 5.

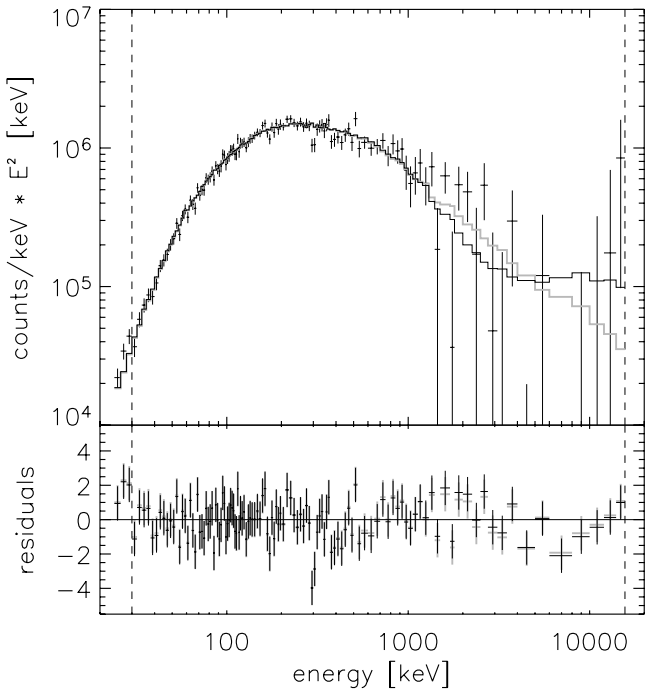

FIG. 3.—Rear spectrum of GRB 020715; error bars: photon counts after background subtraction; black histogram: CBM fit (eq. [10]); gray histogram: Band function fit (eq. [7]); vertical dashed lines: energy range used for fitting; bottom: residuals of CBM (*black*) and Band (*gray*) fits.

Fit.—We had difficulties fitting front and rear spectra consistently below 300 keV. We therefore chose 300 keV as the lower energy bound. The Band function and CBM give the best fits.

We fitted front and rear segments separately, as well as jointly. The results of the joint fit are shown in Figures 4 and 5. For the joint CBM fit we find the 90% confidence level (CL) errors:

$$T_p = 641^{+54}_{-53}\ \text{keV},$$
$$\alpha = 1.523^{+0.099}_{-0.098},$$
$$\beta \equiv 2.1,$$
$$b = 0.0198^{+0.0129}_{-0.0137}. \quad (11)$$

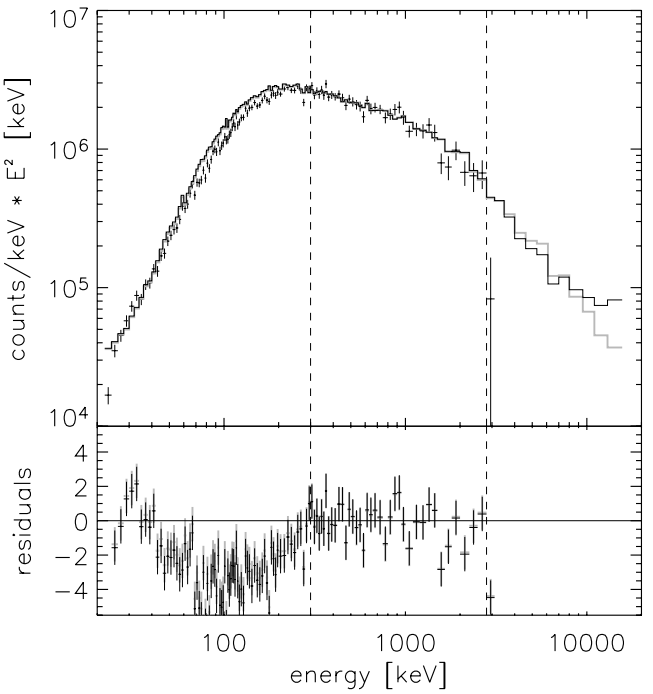

FIG. 4.—Front spectrum of GRB 021008; symbols have same meanings as in Fig. 3; the same set of parameters (eqs. [11] and [12]) is used for this plot and Fig. 5.

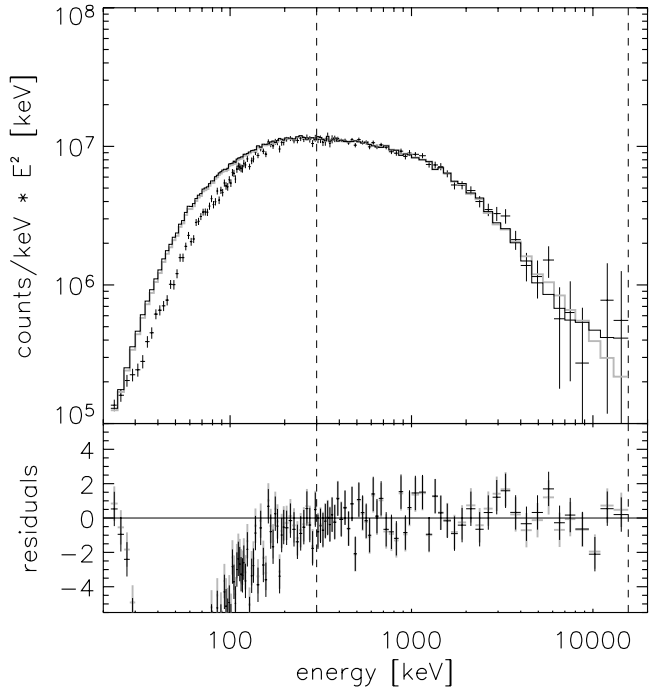

FIG. 5.—Same as Fig. 4, but for the rear spectrum of GRB 021008.

The total χ^2 is 71.2 for $n_{\rm dof} = 74$. The Band function fits marginally better, $\chi^2 = 70.0$ for $n_{\rm dof} = 74$ and its parameters are (90% CL errors)

$$E_p = 677^{+51}_{-66}\ \text{keV},$$
$$\alpha = 1.493^{+0.104}_{-0.104},$$
$$\beta = 3.73^{+0.48}_{-0.38}. \qquad (12)$$

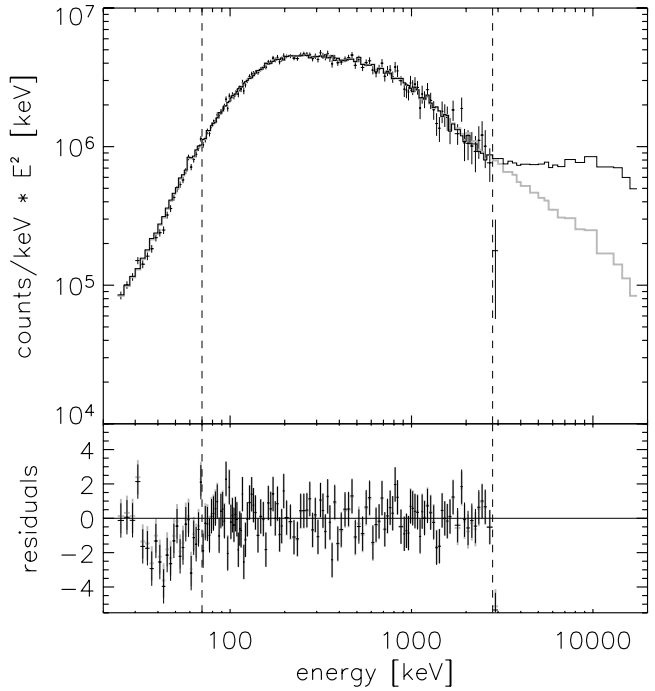

FIG. 6.—Spectrum of GRB 021206, front detectors; symbols have same meanings as in Fig. 3. The same set of parameters (eqs. [13] and [14]) is used for this plot and Fig. 7.

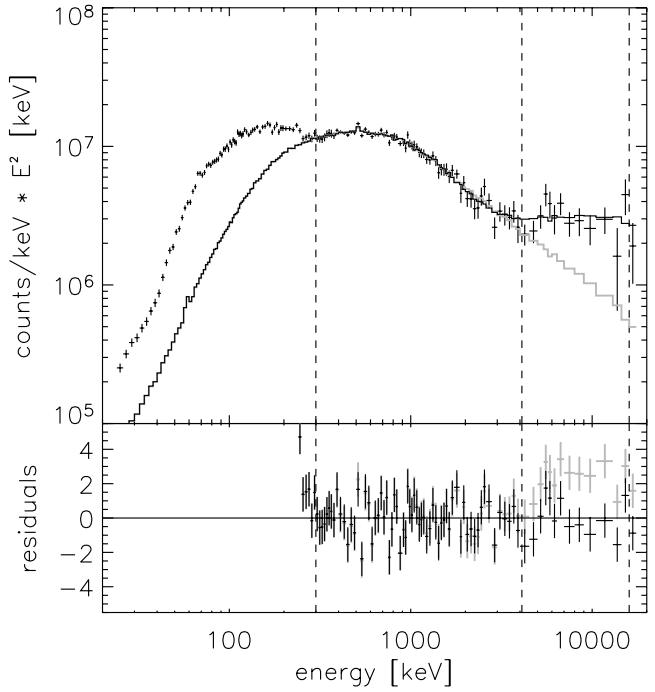

FIG. 7.—*Top*: spectrum of GRB 021206, rear detectors; symbols are the same as in Fig. 3. *Bottom*: residuals of CBM fit (*black*) and Band fit (*gray*). The Band function was fitted only up to 4.5 MeV. The excess counts below 300 keV are backscatters from Earth; see text. The same set of parameters (eqs. [13] and [14]) is used for this plot and Fig. 6.

Discussion.—We do not well understand the spectrum below 300 keV. Both fits, the CBM and the Band function, overestimate the counts below 300 keV. This could be a hint that the GRB spectrum hardens below 300 keV. We find functions that fit the front and the rear data from 40 to 400 keV individually, but they do not agree.

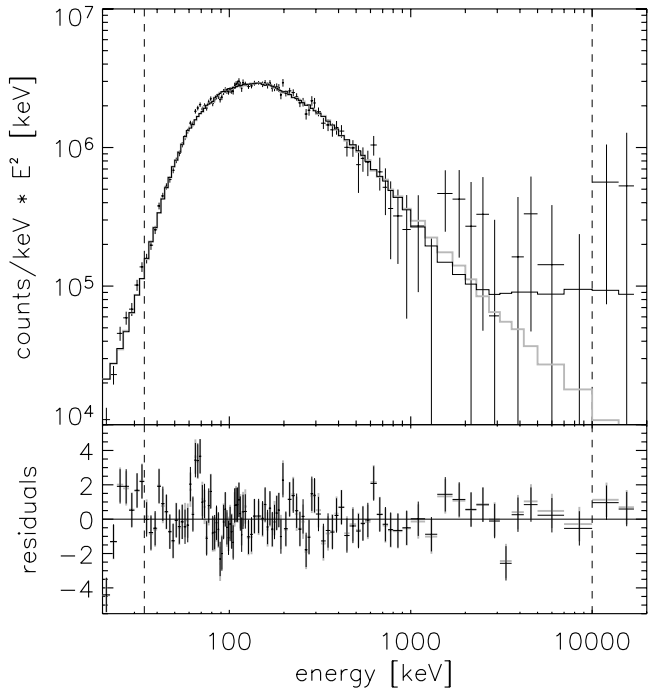

FIG. 8.—Rear spectrum of GRB 030329, first peak; symbols have same meanings as in Fig. 3.

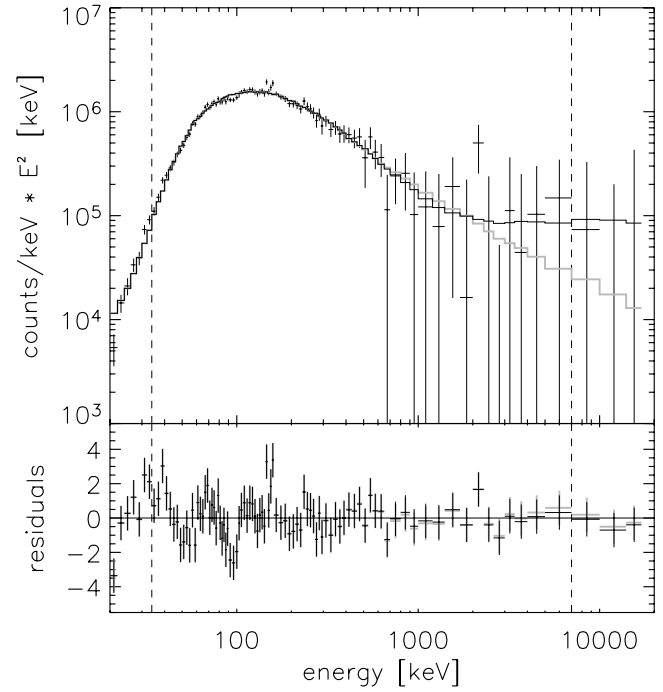

FIG. 9.—Rear spectrum of GRB 030329, second peak; symbols have same meanings as in explanations see caption of Fig. 3.

One possible explanation is the GRB incoming angle of about 50°, at which the GRB photons pass through a certain amount of material before reaching the detectors. Our GEANT simulation tries to take that into account, but it is probably not perfect, and maybe the averaging over all rotation angles is a bad assumption for this short GRB pulse.

Another difficulty for this GRB is its background. For the single rear segments, the background at low energies (below ≈120 keV) strongly depends on the rotation angle of *RHESSI*.

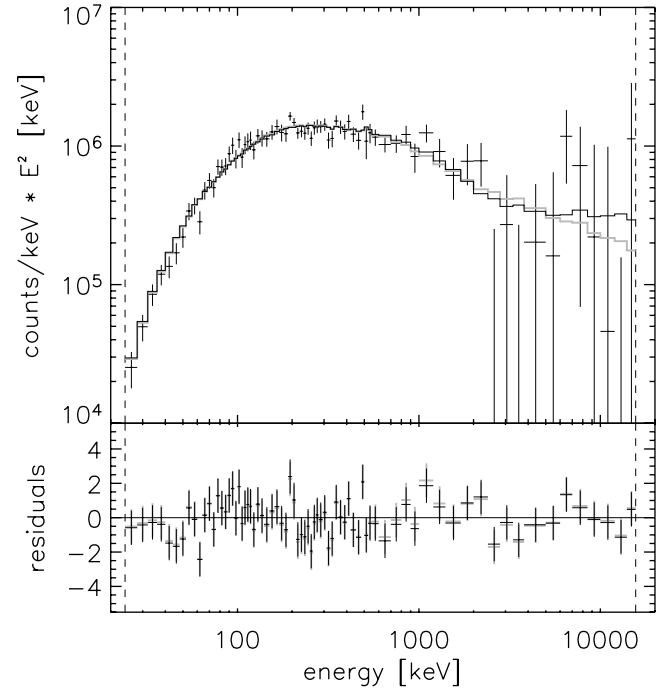

FIG. 10.—Rear spectrum of GRB 030406; symbols have same meanings as in Fig. 3.

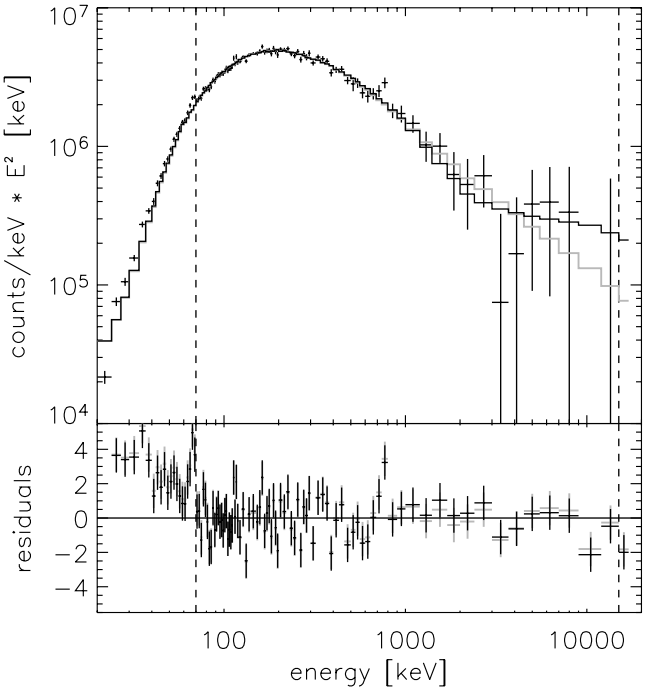

FIG. 11.—Rear spectrum of GRB 030519B; symbols have same meanings as in Fig. 3.

We did our best to take this into account, but maybe we did not succeed completely.

4.3. *GRB 021206*

GRB 021206 is famous for its claimed polarization (Coburn & Boggs 2003), which however turned out to be an artifact (see Rutledge & Fox 2004; Wigger et al. 2004, 2005). This GRB was also studied by Boggs et al. (2004) to probe quantum gravity.

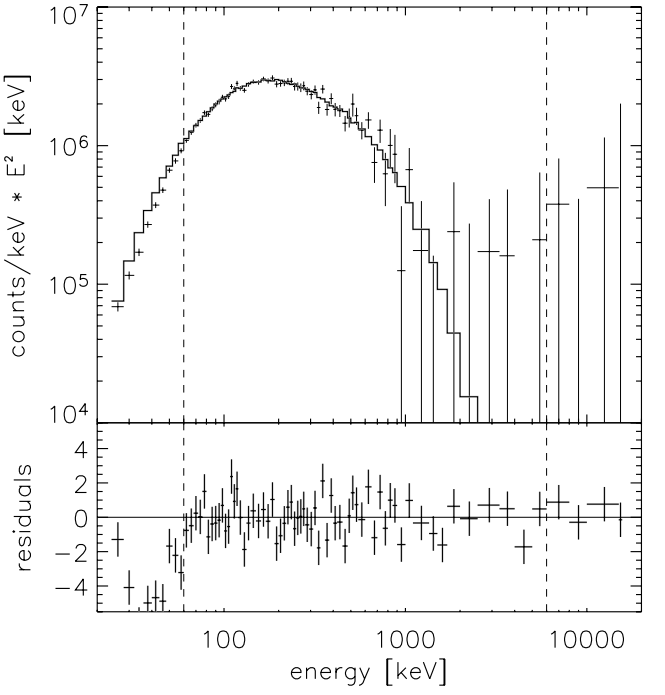

FIG. 12.—Rear spectrum of GRB 031027; histogram and residuals: CPL fit (eq. [5]); a CPL is equivalent to a Band function with $\beta = \infty$ or CBM with $b = 0$.

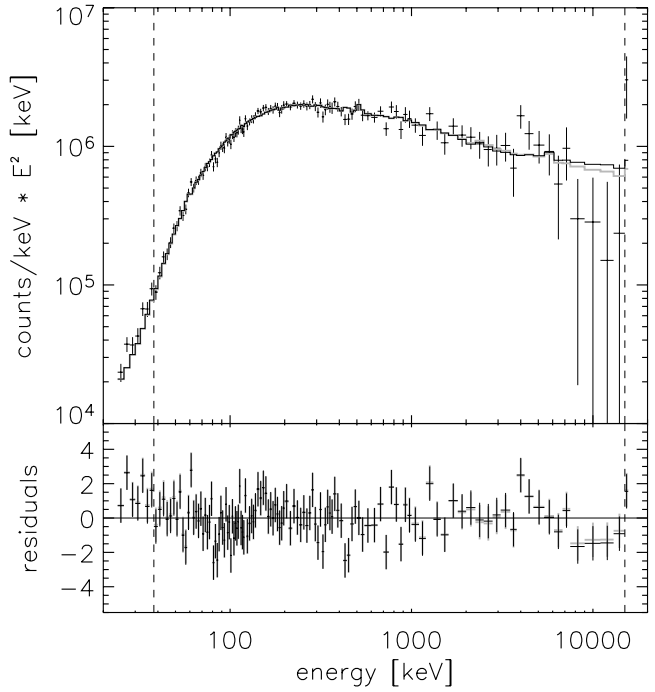

FIG. 13.—Rear spectrum of GRB 031111; symbols have same meanings as in Fig. 3.

This GRB is only 18° from the Sun, exposing mainly the front segments of *RHESSI*'s detectors. Its light curve is shown in Figure 1. Figure 6 shows the energy spectrum in the front segments, Figure 7 in the rear segments.

Fit.—The front spectrum can be fit from 70 keV up to 2800 keV, and the rear from 300 keV to 16 MeV. The huge number of excess counts below 300 keV in the rear detectors is understood: the geometrical constellation of the GRB, *RHESSI*, and Earth was such that the GRB photons came from the front direction, where the effective area is relatively small, whereas the Earth was behind *RHESSI* so the backscattered photons could easily reach the rear segments.

The only function that fits the front *and* rear spectra over the entire energy range from 70 keV up to 16 MeV is the CBM. Fitting front and rear spectra simultaneously with CBM and all parameters free yields (90% CL errors)

$$T_p = 678^{+13}_{-10}\ \mathrm{keV},$$
$$\alpha = 0.60^{+0.09}_{-0.08},$$
$$\beta = 2.12^{+0.08}_{-0.13},$$
$$b = 0.108^{+0.039}_{-0.045}, \qquad (13)$$

with $\chi^2 = 187.5$ for $n_{\mathrm{dof}} = 185$. These values are used for the black line histogram and the residuals in Figures 6 and 7.

The front spectrum alone is well described by a Band function. Its χ^2 is even marginally smaller than that of the CBM model fit (see Table 2). The Band function also fits the rear spectrum up to 4.5 MeV with $\chi^2 = 72.8$ (62 dof), but not at higher energies. The front and rear parameters (up to 4.5 MeV) agree (see Table 4). Evaluating the full parameter space simultaneously for front and rear yields (90% CL errors)

$$E_p = 711^{+15}_{-17}\ \mathrm{keV},$$
$$\alpha = 0.692^{+0.033}_{-0.039},$$
$$\beta = 3.19 \pm 0.08, \qquad (14)$$

with $\chi^2 = 176.5$ for $n_{\mathrm{dof}} = 174$. These values are used for the gray line histogram in Figures 6 and 7. They agree with the preliminary results by Wigger et al. (2007). Above 4.5 MeV, a PL with $\gamma = 2.23 \pm 0.21$ fits the data ($\chi^2 = 12.5$ for 10 dof).

Discussion.—As can be learned from Table 2, the high-energy part cannot be fit by Band, BPL, or CPL, and the low-energy part of the spectrum cannot be fit by BBPL or by BBmPL. The only function that fits over the whole *RHESSI* energy range is CBM.

The CBM function has one more parameter than the Band function. An *F*-test indicates that the chance probability of producing such an improvement in χ^2 with the additional parameter is only 4.0×10^{-9}. The spectral hardening at 4.5 MeV is significant.

Because this GRB has so many counts at high energies, we used a simulation with $\gamma_{\mathrm{sim}} = 1.75$ for the results cited above. A power-law index of 1.75 results in relatively more counts at high energies than the usual power-law index (=2). We also used

TABLE 5
FLUENCES IN 10^{-5} erg cm^{-2}

GRB	F_{CBM} (10^{-5} erg cm^{-2})	F_{Band} (10^{-5} erg cm^{-2})	F_{RHESSI} (10^{-5} erg cm^{-2})	F_{HETE} (10^{-5} erg cm^{-2})	*HETE* (10^{-5} erg cm^{-2})	$F_{Ulysses}$ (10^{-5} erg cm^{-2})	*Ulysses* (10^{-5} erg cm^{-2})
020715	4.37	4.41	3.94	1.93	...	0.43	0.30
021008 front	26.85	26.85	41.24	22.92[a]	...	8.67[a]	...
021008 rear	35.54	35.64	48.85	27.15[a]	...	10.27[a]	8.5
021206 front	52.15	52.44	55.67	19.97	...	3.81	...
021206 rear	58.74	53.45	70.55	25.29	...	4.82	16
030329 P1	6.51	6.47	4.42	5.20	...	2.57	...
030329 P2	3.58	3.58	2.26	2.95	...	1.69	...
030329 total	...	...	7.35	9.46	10.76 ± 0.14	4.93	...
030406	4.81	4.81	4.26	1.62	...	0.40	1.3
030519B	10.27	10.36	9.56	6.07	6.10 ± 0.1	1.78	...
031027	5.37	5.45	4.81	3.97	...	1.17	1.4
031111	7.40	7.40	6.59	2.10	1.714	0.56	0.21

NOTES.—F_{CBM}: fluence from CBM fit (Table 3); F_{Band}: fluence from Band function fit (Table 4); F_{RHESSI}: fluence in [100, 10,000] keV (*RHESSI* range); F_{HETE}: fluence in [30, 400] keV (*HETE* range); $F_{Ulysses}$: fluence in [25, 100] keV (*Ulysses* range); *HETE*: *HETE* fluences from references cited in § 4; *Ulysses*: *Ulysses* fluences from references cited in Table 1.

[a] Our fits overestimate the real counts. More realistic is $F_{Ulysses} = 4.8 \times 10^{-5}$ erg cm^{-2}.

TABLE 6
PEAK RESOLVED ANALYSIS OF GRB 021206

Δt	Duration (s)	T_p (keV)	α	β	b	$F_{\rm CPL}$ (10^{-5} erg cm^{-2})	$F_{\rm mPL}$ (10^{-5} erg cm^{-2})
P1	1.366	661 ± 18	0.77 ± 0.06	2.1	0.059 ± 0.010	11.7	3.0
P2	1.366	732 ± 12	0.42 ± 0.05	2.1	0.115 ± 0.010	14.5	12.9
P3	1.366	684 ± 14	0.63 ± 0.05	2.1	0.085 ± 0.012	12.7	6.3
P4	1.366	530 ± 20	0.80 ± 0.08	2.1	0.113 ± 0.018	6.9	3.8
Tail	4.097	160 ± 60	1.0	2.1	$2.5^{-1.5}_{+\infty}$	0.2	3.1

NOTE.—Δt: time period, cf. Fig. 1; T_p, α, β, and b: CBM parameters; $F_{\rm CPL}$: fluence of the CPL component in the CBM function (eq. [10]); $F_{\rm mPL}$: fluence of the modified PL component of eq. (10); fluences are for the range [100, 10,000] keV.

simulations with $\gamma_{\rm sim} = 1.5$ and 2.0. The results were almost identical, especially for the high-energy parameters β and b of the CBM fit.

The high-energy photon index β of the CBM function agrees perfectly with the theoretical expected value ($\approx$2.1). The low-energy photon index $\alpha \approx 0.6$, on the other hand, is slightly smaller than expected from theory ($\approx$1.0).

Peak resolved analysis.—The time structure of GRB 021206 is rather intricate. Four periods of emission can be distinguished (see Fig. 1), each of them probably consisting of several overlaying subpeaks. Luckily, these time periods match quite well our minimum time resolution of one-third of a rotation period for fitting with a rotation-averaged response function (see § 2.3).

The fitted parameters are listed in Table 6 for the four time intervals marked in the figure, as well as the additional *tail* interval. The *tail* interval lasts one full rotation, starting at the end of the P4 interval. The fluences of the two components in the CBM function (eq. [10]) are listed separately ($F_{\rm CPL}$ for the CPL component and $F_{\rm mPL}$ for the modified PL component). The mPL index β was kept frozen at 2.1.

The energy T_p increases from the first to the second time interval and then decreases. In addition, $F_{\rm CPL}$ and $F_{\rm mPL}$ increase from the first to the second interval, and then decrease. However, the modified PL component seems to decay more slowly than the CPL component. The tail is dominated by the mPL component.

4.4. *GRB 030329*

GRB 030329 is famous for the supernova 2003dh detected in its afterglow (Hjorth et al. 2003; Matheson et al. 2003; Chornock et al. 2003; Zaritsky et al. 2003). The authors of the CBM model used the light curve of this GRB and its early afterglow to predict the later afterglow and the appearance of a supernova (see Dado et al. 2003b). A supernova and the late afterglow were also predicted by Zeh et al. (2003) and are discussed in Ferrero et al. (2006).

In the light curve of GRB 030329, two peaks are clearly separated (Fig. 1, *bottom plot*). We analyze them separately.

Fit.—The spectrum of the first peak is shown in Figure 8. Three bins around a background line from 64 to 70 keV were not included in the fit. A very good fit (see Table 2) is a CPL with $E_{\rm peak} = 158.7 \pm 5.0$ keV and $\alpha = 1.662 \pm 0.032$. Not surprisingly, the CBM and Band function, having more parameters but being closely related to a CPL, fit only marginally better.

The spectrum of the second peak is shown in Figure 9. The spectrum has some wiggles below 160 keV, which account for the relatively high χ^2. Many models give an acceptable fit; only BBPL does not fit. Good fit (see Table 2) is a CPL with $E_{\rm peak} = 78 \pm 13$ keV and $\alpha = 1.83 \pm 0.05$. Another good fit is a broken power law (BPL) with $E_b = 175 \pm 15$ keV, $\alpha = 1.985 \pm 0.032$, and $\beta = 2.68 \pm 0.08$. Also, the Band function and CBM model fit the data well (see Fig. 9).

Discussion.—The prompt emission was detected by *HETE*. Its spectrum is published by Vanderspek et al. (2004) and Sakamoto et al. (2005). Vanderspek et al. (2004) do a time-resolved analysis. For the entire burst they find (90% CL errors) $E_{\rm peak} = 70.2 \pm 2.3$ keV, $\alpha = 1.32 \pm 0.02$, and $\beta = 2.44 \pm 0.08$. Sakamoto et al. (2005) find for the entire burst (90% CL errors) $E_{\rm peak} = 68 \pm 2$ keV, $\alpha = 1.26 \pm 0.02$, and $\beta = 2.28 \pm 0.06$.

The *RHESSI* parameters, for both peaks, are all significantly higher (see Table 4). However, the high-energy photon indices cannot be compared directly, because the break energy (above which β is determined; see eq. [7]) for *HETE* is 116 keV, whereas for *RHESSI* it is >400 keV, i.e., above the *HETE* energy range. Fitting the *RHESSI* data (for the entire duration of the burst) from 135 to 500 keV only, where the *RHESSI* response is good, we find $\beta = 2.441 \pm 0.032$, in excellent agreement with *HETE*. Fitting the *RHESSI* data from 400 to 2000 keV, i.e., above the *HETE* range, we find $\beta = 3.11 \pm 0.25$. The spectrum seems to soften above $\approx$350 keV.

The high *RHESSI* value for α (almost 2.0) for the second light-curve peak indicates that the spectral peak (in the EF_E representation) is broad. Since *RHESSI*'s sensitivity drops below $\approx$80 keV and this is a GRB with $E_{\rm peak}$ of the order of 100 keV, it is likely that *RHESSI*'s α describes the broadness of the peak rather than the low-energy photon index. This opinion is supported by the result of the BPL fit. The low-energy photon index $\alpha \approx 2.0$ shows that the EF_E spectrum is flat from 34 to 175 keV.

It should also be mentioned that the χ^2 of the *HETE* fit, as cited by Sakamoto et al. (2005), is very bad. In addition, the *RHESSI* χ^2 of the spectral fits for the second peak are rather high. A joint fit of *RHESSI* and *HETE* data might reveal interesting features.

4.5. *GRB 030406*

Fit.—The light curve is shown in Figure 2 (*top*) and the spectrum is shown in Figure 10. The best fit is the CBM function with the parameters α and β frozen at the theoretical values. The next best fit is the Band function.

Discussion.—The spectrum of this burst was also studied by Marcinkowski et al. (2006) using data from the *INTEGRAL* satellite. For the spectral analysis, they used combined ISGRI and IBIS Compton mode data. The time interval used by Marcinkowski et al. (2006) differs from ours. Using a time interval similar to that of their "peak" time interval, we find:

1. Fit of a BPL from 24 to 2400 keV (comparable to the energy range in the analysis by Marcinkowski et al. 2006): fits well ($\chi^2 = 70.3$ for $n_{\rm dof} = 60$), and the parameters are $E_b = 479 \pm 80$ keV, $\alpha = 1.08 \pm 0.05$, and $\beta = 1.96 \pm 0.02$.

2. Fit of a BPL from 24 to 16 MeV: does not fit well ($\chi^2 = 86.0$ for $n_{\rm dof} = 71$).

3. Fit of CBM from 24 keV to 16 MeV with $\alpha = 1.0$ and $\beta = 2.1$ frozen: fits well ($\chi^2 = 77.9$ for $n_{\rm dof} = 72$), and the parameters are $T = 1220 \pm 110$ keV and $b = 0.055 \pm 0.079$.

4. Fit of Band function: fits well ($\chi^2 = 77.33$ for $n_{\rm dof} = 71$), and the parameters are $E_{\rm peak} = 1180 \pm 120$ keV, $\alpha = 0.96 \pm 0.06$, and $\beta = 3.02 \pm 0.55$.

For the high-energy part, the parameters found by Marcinkowski et al. (2006) and by us agree. However. we cannot confirm their hard low-energy photon index $\alpha < 0.0$. We even dare to say that we trust our low-energy photon index better, because for this GRB incoming direction, the *RHESSI* response function is well understood, whereas the *INTEGRAL* response function of this burst might suffer from the same systematic effects that we described for *RHESSI* in § 2.4.

4.6. *GRB 030519B*

Fit.—The light curve is shown in Figure 2 and the spectrum in Figure 11. The best fit is the Band function, followed by CBM.

Discussion.—In the *HETE* GRB catalog by Sakamoto et al. (2005) one finds (90% CL errors) $E_p = 138^{+18}_{-15}$ keV, $\alpha = 0.8 \pm 0.1$, and $\beta = 1.7 \pm 0.2$. Since $\beta < 2.0$, the energy E_p is not the peak energy, but only a variable related to the parameter $E_0 = E_p/(2 - \alpha)$. Indeed, the *RHESSI* peak energy for this GRB is >400 keV. But the *HETE* parameters do not fit the *RHESSI* spectrum from 70 to 350 keV ($\chi^2 = 141$ for 53 energy bins).

4.7. *GRB 031027*

The light curve is shown in Figure 2 and the spectrum in Figure 12. The best fit is a cutoff power law with $E_{\rm peak} = 336 \pm 9$ keV and $\alpha = 0.940 \pm 0.05$.

This function is shown in Figure 12. The Band function and CBM have difficulties converging. Since the CPL fits so well, we expect $\beta = \infty$ for the Band function and $b = 0$ for the CBM function.

4.8. *GRB 031111*

Fit.—The light curve is shown in Figure 2 (*bottom*), and the spectrum is shown in Figure 13. The Band function, CBM, and BBmPL are good fits, the best being the Band function.

Discussion.—A preliminary CPL fit to the *HETE* data is published on a Web site[6] as $E_0 = 600.5$ keV and $\alpha = 0.8366$ with a good χ^2. These values describe the *RHESSI* spectrum well from 80 to 350 keV, but not at higher energies. *HETE*'s energy range ends at 400 keV; thus, we believe that our values for E_0 and α are better.

5. GENERAL DISCUSSION AND CONCLUSION

5.1. *The Spectral Functions*

What is an acceptable χ^2? In the limit of many degrees of freedom ($n_{\rm dof} > 30$), χ^2 is normal distributed with an expectation value of $n_{\rm dof} - 0.5$ and a variance of $\sigma_{\chi^2} = (2n_{\rm dof} - 1)^{1/2}$. A fit is acceptable if χ^2 is close to its expectation value *and* if the residuals scatter around zero over the whole fit range, i.e., if the fit "looks good."

From Table 2 we conclude that the CBM gives acceptable χ^2 for *all* GRBs studied. And they also look good, as can be seen in Figures 3–13. Except for GRB 021206, rear (Fig. 7), the same can be said for the Band function.

[6] See http://space.mit.edu/HETE/Bursts/GRB031111A/.

In many cases, a cutoff power law (CPL) fits the spectrum up to high energies, e.g., GRB 021008, GRB 030329, or GRB 031027. In these cases, Band and CBM improve the goodness of fit slightly, but all three spectral shapes fit the data acceptably.

A broken power law fits sometimes, but usually not well. BBPL and BBmPL do not fit in general; BBPL fits worse than BBmPL. However, it should be mentioned that a blackbody component is expected—if at all—only at the beginning of a GRB (see, e.g., Ryde et al. 2006, and references therein), whereas we fitted the entire duration of the bursts. When using BBPL, we often find that the PL component fits either at high energies or at low energies. This is also discussed by Ghirlanda et al. (2007), who studied six BATSE GRBs in detail, where low-energy data from the WFC instrument (on board *BeppoSAX*) are available. They find that the WFC data fit the Band function or CPL extrapolation, but not the BBPL extrapolation to low energies. Arguing that the PL contribution is too simple, they try to fit a blackbody spectrum plus CPL. We suggest using our BBmPL function instead. Its modified PL component describes a spectral break from $dN/dE \propto E^{-(\beta-1)}$ at low energies to $dN/dE \propto E^{-\beta}$ at high energies.

5.2. *CBM Function*

The present work is, to our knowledge, the first systematic attempt to fit the CBM function to prompt GRB spectra. The two terms in equation (10) have a simple meaning. According to the cannonball theory, all GRBs are associated with a supernova. The ambient light is Compton up-scattered by the cannonball's electrons, producing the prompt GRB emission. Some electrons are simply comoving with the cannonball, giving rise to the CPL term in equation (10). Since the photon spectrum of the ambient light can be described by a thin thermal bremsstrahlung spectrum, α is expected to be $\approx$1. The second term (mPL) is caused by a small fraction of electrons accelerated to a power-law distribution, resulting in a photon index of $\beta \approx 2.1$ (see, e.g., Dado & Dar 2005, their § 3.8, or Dado et al. 2007, their §§ 2 and 4.1 for a summary).

In our study, the observed values for α are all approximately 1, as predicted by the CBM. Because of the low count statistics at high energies, we could not always fit β. We then fixed it to its theoretical value of 2.1 in order to make the fit converge and to obtain a value for the parameter b. In the cases where we could fit β, we found values close to 2.1 (Table 3).

For the factor b of the modified PL component in the CBM function we typically found values of the order of 0.1. An exception is GRB 031111, where b is of the order of 1.0, but with a large error (0.4).

Our values for β and b are similar to those found by Dado & Dar (2005; fit of GRB 941017) and by Dado et al. (2004; fit of *X*-ray flashes XRF 971019, XRF 980128, and XRF 990520 using *BeppoSAX*/WFC and CGRO/BATSE data). The authors of the CBM hypothesize that XRFs are simply GRBs viewed further off the jet axis.

The different time development of the CPL and the mPL fluences, as reported in Table 6, possibly points to a different time dependence of the two underlying electron distributions within a cannonball.

5.3. *Fitting CBM Function versus CPL and Band Function*

Both the Band function and the CBM function are extensions of a CPL, the Band function with one additional parameter, the CBM function with two. For cases for which a CPL fits the data well, a Band function with $\beta = \infty$ or a CBM function with

$b = 0$ (and $\beta = 2.1$ or any other value) also fits. This is the case for GRB 031027.

Whether additional parameters are necessary in a fit can be tested with the *F*-test. For GRB 030329, the extra parameters are barely needed. For GRB 020715, 021008, 021206, 030406, 030519B, and 031111 additional parameters are required at a confidence level of at least 90%.

Concerning the question of whether the high-energy power-law parameter β in the CBM should be treated as a free parameter, the answer is "yes" from a theoretical point of view, but in practice (see Table 2), the improvements in χ^2 are marginal or small for all bursts that we studied. Our practice of freezing β at its theoretically predicted value in cases of bad convergence seems to be acceptable.

It is more difficult to compare the goodness of fit of the Band versus the CBM function. The two functions are not independent, because they both are dominated by a CPL up to the peak energy and higher. In most cases of our study, the two functions fit the observed spectrum equally well with a slight preference for the Band function. At high energies, however (typically above several times the peak energy), the two functions are different, the spectral hardening being a unique feaure of the CBM function. There is only one case, namely, GRB 021206, where this hardening is observed. For the rear data going up to high energies, a Band function fit gives $\chi^2/\mathrm{dof} = 133.3/74$ (see Table 2). This is not acceptable at $<0.01\%$ probability of being accidentally so high. The CBM fit, on the other hand, gives $\chi^2/\mathrm{dof} = 82.7/73$, which is fully acceptable at a 20% level.

We would like to stress again that, while the CBM gives acceptable fits for *all* cases, the Band function fails in one case. This seems enough to us to give some credit to the CBM.

However, it is, of course, no proof that the CBM is the only theory capable of describing the spectrum of GRB 021206. For example, a Band function plus a PL with $\gamma \approx 1.5$ would also fit. But there is no theory to predict such a shape. To our knowledge, CBM is to date the only existing GRB model that explains the prompt GRB spectra from first principles.

At this point we also would like to note that the mean α-value found for the BATSE catalog is 1 (see Kaneko et al. 2006). We cite from their summary: "*We confirmed, using a much larger sample, that the most common value for the low-energy index is* ≈ -1 (Preece et al. 2000; Ghirlanda et al. 2002).[7] The overall distribution of this parameter shows no clustering or distinct features at the values expected from various emission models, such as $-2/3$ for synchrotron (Katz 1994; Tavani 1996), 0 for jitter radiation (Medvedev 2000), or $-3/2$ for cooling synchrotron (Ghisellini & Celotti 1999)." They do not mention the CBM which would explain $\alpha \approx 1$.

Note that the β-values of the CBM are systematically lower than the β-values of the Band function (cf. Tables 3 and 4). From Band function fits to BATSE GRBs, it is known that β is clustered around 2.3, with a long tail toward higher values (see Kaneko et al. 2006). For CBM we would expect β to cluster at slightly lower values. For criticism of the CBM, see, e.g., Hillas (2006), but see also the answer by Dar & de Rújula (2006).

5.4. *The Spectral Hardening*

The difference between a CBM spectrum and the Band function is the hardening at high energies. This becomes visible—for the GRBs studied here—in the few MeV region, but it depends on the peak energy and the factor b. For $\alpha = 1.0$ and $b = 0.10$ the hardening typically appears at several times the peak energy and the second term dominates at 10 times the peak energy. For the spectral fit of XRFs done by Dado et al. (2004) the spectral hardening is expected in the few hundred keV region, just where the number of photons detected runs low. Most of our GRBs also suffer from this lack of statistics at high energies, preventing the detection of a hardening.

A spectral coverage of two decades and good detection efficiency at high energies is necessary to experimentally observe the full shape of the CBM function. In the case of GRB 021206 we were able to detect this hardening, thanks to *RHESSI*'s broad energy range (30 keV–15 MeV) and the fact that this is one of the brightest GRBs ever observed.

There is a GRB observed by *SMM* from 20 keV up to 100 MeV, namely, GRB 840805. As reported by Share et al. (1986) the spectrum of this burst shows emission up 100 MeV. In order to fit the spectrum, "a classical thermal synchrotron function plus a power law" was used. The power-law component was required to fit the data above about 6 MeV. This is a hint of a spectral hardening around 6 MeV, and we suppose that the spectrum of this GRB can be fit by a CBM function.

The spectral hardening observed in GRB 941017 (González et al. 2003) seems to be different. The photon index of GRB 941017 above a few MeV is $\approx$1.0. This case is discussed by Dado & Dar (2005) as a possible additional feature in the CBM spectrum.

5.5. *Outlook*

In order to find more GRB spectra that show the hardening characteristic for the CBM function, strong GRBs have to be observed over a broad enough energy range. With the forthcoming *GLAST* mission, we expect that more such spectra will be observed. However, joint analyses with more than one instrument could also reveal this hardening. We therefore suggest

1. Searching for CBM spectrum candidates among joint *Swift*/*RHESSI* GRBs and XRFs, and joint *Swift*/Konus GRBs.
2. Reanalyzing some BATSE bursts. Looking at the BATSE spectra published by Ghirlanda et al. (2007), we suppose that the CBM can possibly improve the fits of GRB 980329, GRB 990123, and GRB 990510. The same can be said for GRB 911031 as published by Ryde et al. (2006). And GRB 000429, as published in Figure 19 of Kaneko et al. (2006), looks like a promising candidate as well.
3. Searching in Konus data for suitable GRBs.
4. Adding the CBM function to XSPEC in order to make it more accessible to the astronomical community.

6. SUMMARY

We have presented the time-integrated spectra of 8 bright GRBs observed by *RHESSI* in the years 2002 and 2003. The spectrum of GRB 021206 shows a hardening above 4 MeV. From 70 keV to 4.5 MeV, the spectrum can be well fitted by a Band function—but not above that. The cannonball model successfully describes the entire spectrum up to 16 MeV, the upper limit of *RHESSI*'s energy range. For the spectra of the seven other GRBs analyzed, we found that they can be fitted by the CBM, as well as by the Band function. We therefore suggest that the cannonball model should be considered for fitting GRB spectra.

We thank K. Hurley, A. Kann, S. McGlynn, J. Řipa, and L. Hanlon for helpful discussions and comments.

[7] This corresponds to +1 in our notation.

REFERENCES

Band, D., et al. 1993, ApJ, 413, 281
Barlow, R., & Beeston, C. 1993, Comput. Phys. Commun., 77, 219
Boggs, S. E., Wunderer, C. B., Hurley, K., & Coburn, W. 2004, ApJ, 611, L77
CERN. 1993, GEANT: Detector Description and Simulation Tool, CERN Program Library Long Writeup W5013 (Geneva: CERN), http://wwwusdoc.web.cern.ch/wwwasdoc/pdfdir/geant.pdf
Chornock, R., et al. 2003, GCN Circ. 2131, http://gcn.gsfc.nasa.gov/gcn/gcn3/2131.gcn3
Coburn, W., & Boggs, S. E. 2003, Nature, 423, 415
Dado, S., & Dar, A. 2005, ApJ, 627, L109
Dado, S., Dar, A., & de Rújula, A. 2002, A&A, 388, 1079
———. 2003a, A&A, 401, 243
———. 2003b, ApJ, 594, L89
———. 2004, A&A, 422, 381
———. 2007, preprint (arXiv:0706.0880v1)
Dar, A., & de Rújula, A. 2004, Phys. Rep., 405, 203
———. 2006, preprint (hep-ph/0611369v1)
Ferrero, P., et al. 2006, A&A, 457, 857
Ghirlanda, G., et al. 2002, A&A, 393, 409
———. 2003, A&A, 406, 879
———. 2007, MNRAS, 379, 73
Ghisellini, G., & Celotti, A. 1999, A&AS, 138, 149
González, M. M., et al. 2003, Nature, 424, 749
Hillas, A. M. 2006, preprint (arXiv:astro-ph/0607109v2)
Hjorth, J., et al. 2003, Nature, 423, 847
Hurley, K., et al. 2002a, GCN Circ. 1454, http://gcn.gsfc.nasa.gov/gcn/gcn3/1454.gcn3
———. 2002b, GCN Circ. 1456, http://gcn.gsfc.nasa.gov/gcn/gcn3/1456.gcn3
———. 2002c, GCN Circ. 1617, http://gcn.gsfc.nasa.gov/gcn/gcn3/1617.gcn3
———. 2002d, GCN Circ. 1629, http://gcn.gsfc.nasa.gov/gcn/gcn3/1629.gcn3
———. 2002e, GCN Circ. 1727, http://gcn.gsfc.nasa.gov/gcn/gcn3/1727.gcn3
———. 2002f, GCN Circ. 1728, http://gcn.gsfc.nasa.gov/gcn/gcn3/1728.gcn3
———. 2003a, GCN Circ. 2127, http://gcn.gsfc.nasa.gov/gcn/gcn3/2127.gcn3
———. 2003b, GCN Circ. 2281, http://gcn.gsfc.nasa.gov/gcn/gcn3/2281.gcn3
Hurley, K., et al. 2003c, GCN Circ. 2237, http://gcn.gsfc.nasa.gov/gcn/gcn3/2237.gcn3
———. 2003d, GCN Circ. 2438, http://gcn.gsfc.nasa.gov/gcn/gcn3/2438.gcn3
———. 2003e, GCN Circ. 2443, http://gcn.gsfc.nasa.gov/gcn/gcn3/2443.gcn3
Kaneko, Y., et al. 2006, ApJS, 166, 298
Katz, J. I. 1994, ApJ, 432, L107
Lamb, D., et al. 2003, GCN Circ. 2235, http://gcn.gsfc.nasa.gov/gcn/gcn3/2235.gcn3
Lin, R. P., et al. 2002, Sol. Phys., 210, 3
Marcinkowski, R., et al. 2006, A&A, 452, 113
Matheson, T., et al. 2003, GCN Circ. 2120, http://gcn.gsfc.nasa.gov/gcn/gcn3/2120.gcn3
McBreen, S., et al. 2006, A&A, 455, 433
Medvedev, M. V. 2000, ApJ, 540, 704
Preece, R. D., et al. 2000, ApJS, 126, 19
———. 2002, ApJ, 581, 1248
Rutledge, R. E., & Fox, D. B. 2004, MNRAS, 350, 1288
Ryde, F. 2004, ApJ, 614, 827
Ryde, F., et al. 2006, ApJ, 652, 1400
Sakamoto, T., et al. 2005, ApJ, 629, 311
Share, G. H., et al 1986, Adv. Space Res., 6, 15
Smith, D. M., et al. 2002, Sol. Phys., 210, 33
Tavani, M. 1996, ApJ, 466, 768
Wigger, C., et al. 2004, ApJ, 613, 1088
———. 2005, Nuovo Cimento C, 28, 265
———. 2007, Nouvo Cimento B, 121, 1117
Vanderspek, R., et al. 2003, GCN Circ. 1997, http://gcn.gsfc.nasa.gov/gcn/gcn3/1997.gcn3
———. 2004, ApJ, 617, 1251
Zaritsky, D., Bolte, M., Garnavich, P. M., Bonanos, A., & Stanek, K. Z. 2003, GCN Circ. 2169, http://gcn.gsfc.nasa.gov/gcn/gcn3/2169.gcn3
Zeh, A., Klose, S., & Greiner, J. 2003, GCN Circ. 2081, http://gcn.gsfc.nasa.gov/gcn/gcn3/2081.gcn3